Available online at www.sciencedirect.com
SCIENCE DIRECT
Journal of Power Sources 158 (2006) 36–44
JOURNAL OF POWER SOURCES
www.elsevier.com/locate/jpowsour

Colloidal Au and Au-alloy catalysts for direct borohydride fuel cells: Electrocatalysis and fuel cell performance

Mohammed H. Atwan [a], Charles L.B. Macdonald [b], Derek O. Northwood [a,*], Elod L. Gyenge [c,*]

[a] *Department of Mechanical, Auto and Materials Engineering, University of Windsor, Windsor, Canada N9B 3P4*
[b] *Department of Chemistry and Biochemistry, University of Windsor, Windsor, Canada N9B 3P4*
[c] *Department of Chemical and Biological Engineering, The University of British Columbia, Vancouver, BC, Canada V6T 1Z4*

Received 14 July 2005; accepted 1 September 2005
Available online 17 November 2005

Abstract

Supported colloidal Au and Au-alloys (Au-Pt and Au-Pd, 1:1 atomic ratio) on Vulcan XC-72 (with 20 wt% metal load) were prepared by the Bönneman method. The electrocatalytic activity of the colloidal metals with respect to borohydride electro-oxidation for fuel cell applications was investigated by voltammetry on static and rotating electrodes, chronoamperometry, chronopotentiometry and fuel cell experiments. The fundamental electrochemical techniques showed that alloying Au, a metal that leads to the maximum eight-electron oxidation of BH_4^-, with Pd or Pt, well-known catalysts of dehydrogenation reactions, improved the electrode kinetics of BH_4^- oxidation. Fuel cell experiments corroborated the kinetic studies. Using 5 mg cm^{-2} colloidal metal load on the anode, it was found that Au-Pt was the most active catalyst giving a cell voltage of 0.47 V at 100 mA cm^{-2} and 333 K, while under identical conditions the cell voltage using colloidal Au was 0.17 V.

Keywords: Borohydride fuel cells; Colloidal metals; Electrocatalysis

1. Introduction

Borohydride fuel cells are currently under active investigation as part of worldwide efforts to develop environmentally sustainable sources of power [1–5]. The so-called direct borohydride fuel cell (DBFC) variant relies on the anodic oxidation of BH_4^- as opposed to the use of the borohydride solution as a H_2 storage media connected to the H_2–O_2 fuel cell. The potential advantages of the direct BH_4^- oxidation pathway are mainly related to system simplicity (e.g., a separate heterogeneous reactor for H_2 generation [6] is not required) and easier adaptability to micro-scale (portable power) applications. Among the disadvantages of the direct borohydride fuel cell option are: the BH_4^- crossover to the cathode [7] and an insufficient understanding at present of the BH_4^- electro-oxidation kinetics and associated catalytic aspects. From the fuel cell power output point of view, at the moment the literature is lacking of conclusive studies comparing the two variants under identical operating conditions.

The electrochemical reactions in a DBFC equipped with a cation exchange membrane (e.g., Nafion®) to minimize the BH_4^- crossover are:

$$\text{Anode}: \quad NaBH_4 + 8NaOH \rightarrow NaBO_2 + 6H_2O + 8e^- + 8Na^+, \quad E^\circ = -1.24\,V_{SHE}, \tag{1}$$

$$\text{Cathode}: \quad 2O_2 + 4H_2O + 8e^- + 8Na^+ \rightarrow 8NaOH, \quad E^\circ = 0.40\,V_{SHE}. \tag{2}$$

The overall fuel cell reaction is:

$$NaBH_4 + 2O_2 \rightarrow NaBO_2 + 2H_2O, \quad E^\circ_{cell} = 1.64\,V. \tag{3}$$

Thus far, very few anode materials were identified that favor the complete eight-electron oxidation according to Eq. (1). It has been conclusively established that the electro-oxidation of BH_4^- on Au is virtually an eight-electron process [8,9]. Out of the total eight electrons transferred there is some information,

* Corresponding author. Tel.: +1 604 822 3238; fax: +1 604 822 6003.
E-mail addresses: dnorthwo@uwindsor.ca (D.O. Northwood), egyenge@chml.ubc.ca (E.L. Gyenge).

0378-7753/$ – see front matter © 2005 Elsevier B.V. All rights reserved.
doi:10.1016/j.jpowsour.2005.09.054

obtained by Bard and co-workers employing scanning electrochemical microscopy, with regard to the mechanism involving the first two electron transfer steps occurring in a ECE sequence [8]. The rest of the mechanistic details are unknown at present.

Amendola and co-workers evaluated Au (97%)-Pt (3%) electrodeposited on carbon cloth (particle diameter roughly about 500 nm, with agglomerates up to about 4 μm) as anode in a direct borohydride fuel cell equipped with anion exchange membrane. A cell voltage of 0.5 V was obtained at 123.9 mA cm^{-2} and 343 K [4]. Unfortunately, the catalyst load was not specified.

On the vast majority of metals and alloys studied in relation to BH_4^- oxidation (e.g., Ni, Pt, Pd, Ni_xB) the complete eight-electron exchange is not achieved. Furthermore, on metals leading to the incomplete oxidation of borohydride the faradaic reaction is typically accompanied by the catalytic hydrolysis of BH_4^- yielding H_2 and a number of potential boronhydroxide (or oxide) intermediates. One possible hydrolysis pathway could be summarized as:

$$NaBH_4 + yH_2O \rightarrow NaBH_{4-y}(OH)_y + yH_2, \quad \text{with } y = 1, \ldots, 4. \tag{4}$$

The goal of the present study was to prepare colloidal Au and Au-alloy particles supported on carbon and to investigate them for electrocatalytic activity with respect to BH_4^- oxidation by carrying out both fundamental electrochemical techniques and fuel cell experiments. This is the first investigation to the authors' knowledge, looking at colloidal metal catalysts for BH_4^- electro-oxidation.

2. Experimental methods

2.1. Colloidal metal preparation technique

The colloidal metal synthesis has been described in detail in our previous publications [5,10]. The so-called Bönneman method was employed with the modifications introduced by Götz and Wendt [11,12]. All the colloidal metals were prepared with a 20 wt% metal load on Vulcan XC72R support (L.V. LAMOS Limited). In the case of the alloys the Au to co-catalyst atomic ratio was 1:1 in all cases.

A 50% excess (4.5, 7.5 and 7.5 ml) of 0.5 M of tetrabutylammoniumtriethyl hydroborate, $N(C_4H_9)_4[B(C_2H_5)_3H]$, was added dropwise over a period of 1 h at 296 K to a stirred suspensions in 100 ml THF of anhydrous salts of $AuCl_3$ (STREM Chemical Inc., 99.9%, anhydrous) (0.151 g, 0.5 mmol), $AuCl_3$ (0.151 g, 0.5 mmol) and $PtCl_2$ (STREM Chemical Inc., 99.9%, anhydrous) (0.1329 g, 0.5 mmol), $AuCl_3$ (0.151 g, 0.5 mmol) and $PdCl_2$ (STREM Chemical Inc., 99.9%, anhydrous) (0.0886 g, 0.5 mmol), respectively. Almost complete dissolution of the salt(s) occurred after stirring the deep dark coloured solution for 4 h. To destroy any unreacted reducing agent, 5 ml of acetone was added and stirred for 1 h. The solution then was added dropwise to a stirred suspension of the carbon support (Vulcan XC72R) in 100 ml THF. The mixture was stirred for 12 h. 150 ml of ethanol (Sigma–Aldrich, 99.5%, anhydrous) was then added and stirred for 2 h. After filtering the reaction solution through D-4 glass frit, the supported catalyst(s) was washed with ethanol several times, and then dried under a nitrogen vacuum at 296 K for 12 h.

Annealing and reducing processes were done to remove the protecting organic shell in order to enhance the catalytic activity. These processes were performed in three stages using a tubular furnace. First, the samples were treated at 573 K for 30 min under N_2 at a flow rate of 160 ml min^{-1}. In this step most of the organic shell is decomposed. Second, annealing was performed in a N_2/O_2 mixture (10 vol.% O_2) at a flow rate of 160 ml min^{-1} for 30 min at 573 K. In the third and last step, the samples were subjected to a reducing environment using 100 vol.% H_2 at a flow rate of 160 ml min^{-1} for 30 min at 573 K, in order to reduce any oxidized metal(s) during the annealing processes. Nitrogen was purged for 5 min before and after the annealing process to avoid any contact between oxygen and hydrogen gases.

Fig. 1 shows the powder energy dispersive spectrometry (EDS) spectra for Au and Au-alloys corresponding to a selected zone in the powder sample indicated in the inset. EDS spectra was also obtained for the 'blank' Vulcan XC72R support. In addition to the metals and the carbon from the support, the samples contained trace amounts of sulfur, which originated from the Vulcan XC72R. However, typically the post-preparation sample washing and treatment methods were effective in eliminating the LiCl by-product, consequently adsorbed LiCl was not detected by EDS. Fig. 2 shows the X-ray diffraction spectra for the catalysts under consideration, revealing the [1 1 1], [2 0 0], [2 2 0] and [3 1 1] reflections of the fcc metallic lattice for Au, Au-Pt and Au-Pd, respectively.

The Bönneman colloid method produces nanoparticles sizes of 1.3, 2.5, 2.8 and 10 nm for Ru, Pd, Pt and Au, respectively [11]. The particle sizes of binary alloys were found to be roughly close to the average between the individual metal particle sizes (e.g., for Pt-Ru (1:1 atomic ratio) the mean diameter was 1.7 nm [12]). Therefore, it is estimated that the diameter of the Au-Pt and Au-Pd particles is about 6 nm.

2.2. Fundamental electrochemical methods

To carry out the electrochemical investigation the supported metal colloids were fixed on a glassy carbon (GC) disk electrode of 3 mm diameter manufactured from a glassy carbon rod (Electrosynthesis Inc.) inserted tightly in a hollow Teflon cylinder and sealed by thermal treatment. An amount of 5 mg carbon supported catalyst powder (20 wt% metal) was dispersed by sonication for 45 min in 1 ml solution composed of 0.25 ml Nafion solution 5 wt% (Sigma–Aldrich Inc.) and 0.75 ml ethanol (Sigma–Aldrich Inc.). From the suspension of supported catalyst 10 μl was carefully applied on the GC electrode surface yielding for each of the investigated catalysts a constant load per metal basis of 141 μg cm^{-2}. The dispersed catalyst on GC substrate was dried in a mild N_2 stream for about 1 h creating a good bonding and electronic contact between the supported catalyst and the GC electrode.

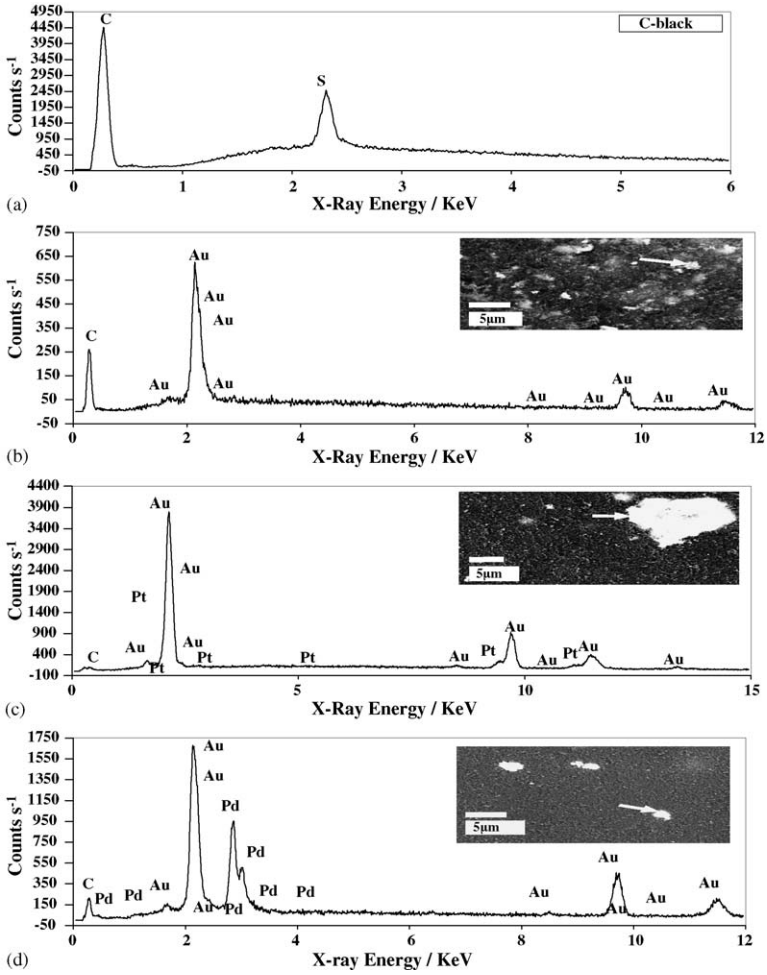

Fig. 1. Powder energy dispersive spectrometry (EDS) spectra. (a) Vulcan XC72, (b) Au, (c) Au-Pt and (d) Au-Pd.

Electrochemical tests were performed using the conventional three-electrode arrangement composed of the dispersed colloidal metal supported on GC working electrode, two graphite rods with an area of about 10 cm^2 each, placed on the opposite sides of the cell acting as the counter electrodes, and a Hg/HgO electrode in 2 M NaOH (Radiometer Analytical S.A.) acting as reference. The potential of the Hg/HgO electrode (abbreviated as MOE) was −0.068 V with respect to a Ag/AgCl, KCl_{std} reference.

Cyclic voltammetry, chronoamperometry and chronpotentiometry experiments were conducted at 295 K employing either a PAR 263A or a PARSTAT 2263 computer controlled potentiostat (Princeton Applied Research Inc.) and the associated Power Sweep and Power Step software (part of the Power Suite package). Voltammetry on rotating disc electrode (RDE) experiments were performed using the Volta Lab 80 (PGZ402, Radiometer Analytical S.A.) in conjunction with the glassy carbon electrode tip (A35T090, Radiometer Analytical S.A., diameter 3 mm), RDE (EDI101, Radiometer Analytical S.A.) and speed control unit (CTV101, Radiometer Analytical S.A.). The supporting electrolyte was 2 M NaOH. The employed $NaBH_4$ (Alfa Aesar Inc., purity + 97 wt%) concentrations were between 0.03 and 1 M.

2.3. Borohydride fuel cell with solid polymer electrolyte

Tests on direct borohydride fuel cells were performed using the Fideris Inc. FCTS MTK system controlled with the FC Power software. Membrane electrode assemblies (MEAs) of 5 cm^2 effective geometric area were prepared by applying the synthesized colloidal catalysts on a carbon cloth (Electrochem. Inc.), followed by hot pressing of the cloth to the anode side of a half-MEA with Nafion® 117 membrane supplied by Electrochem Inc. where the cathode side consisted of 4 mg cm^{-2} Pt and Toray Carbon paper gas diffusion layer.

The MEA preparation procedure consisted of the following steps: 5 mg cm^{-2} on metal(s) basis of the colloidal catalyst was mixed with 1 mg cm^{-2} Nafion® 117 (i.e., applied as the corresponding volume of a Nafion 5 wt% solution) and 0.7 ml ethanol. The mixture was placed in an ultrasonic bath for 45 min. Afterwards, the supported catalyst suspension was applied on the carbon cloth by a technique similar to the decal method, followed by drying in a N_2 atmosphere for 12 h. The final stage in the MEAs preparation was the hot pressing of the anode catalyst layer together with another carbon cloth acting as the anodic backing layer onto the Nafion® 117 membrane

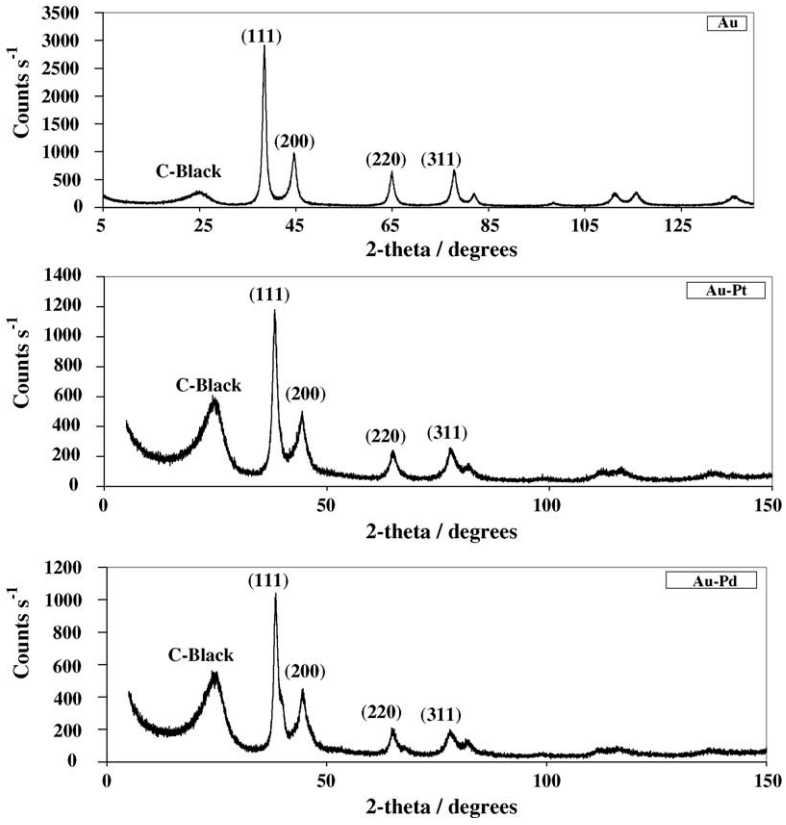

Fig. 2. X-ray diffraction pattern of 20 wt% (1:1 atomic ratio) colloidal Au and Au-alloys.

with the commercial cathode side. Hot pressing was performed at 545 kg for 2 min at 433 K. After hot pressing, the full MEA was assembled together with the end plates in the fuel cell test station. Membrane conditioning was performed by recirculating a solution of 2 M NaOH at 60 ml min^{-1} for 2 h prior to each test. The pure sodium hydroxide solution was then replaced by a 2 M $NaBH_4$ in 2 M NaOH solution at feed rates of 20, 50 and 85 ml min^{-1}. The oxygen flow rate was fixed at 200 ml min^{-1} for all tests, with an absolute pressure of 2.7 atm. The tests were started after the fuel cell temperature and the fuel feed flow stream temperatures reached either 298 or 333 K, respectively. The potential versus current data were recorded.

3. Results and discussion

3.1. Voltammetry of borohydride oxidation on static electrodes

Figs. 3–5 show the linear voltammograms on static electrodes for colloidal Au, Au-Pt and Au-Pd as a function of $NaBH_4$ concentration between 0.03 and 1 M. The scan rate was 100 mV s^{-1}. On colloidal Au (Fig. 3) a wide oxidation wave can be identified between −0.6 and +0.4 V versus MOE, as a function of borohydride concentration. This wave is consistent with previously reported BH_4^- voltammograms obtained on a flat Au surface due to the overall eight-electron oxidation of BH_4^- (Eq. (1)) [9].

Alloying Au, a fairly inert catalyst for dehydrogenation reactions [13], with metals that are widely used for oxidative dehydrogenation processes, such as Pt and Pd, could be of interest to enhance the catalytic activity toward the electro-oxidation of $NaBH_4$. The aim is to combine the high coulombic efficiency of eight-eletron transfer on Au with the well-known catalytic effect of Pt or Pd for dehydrogenation.

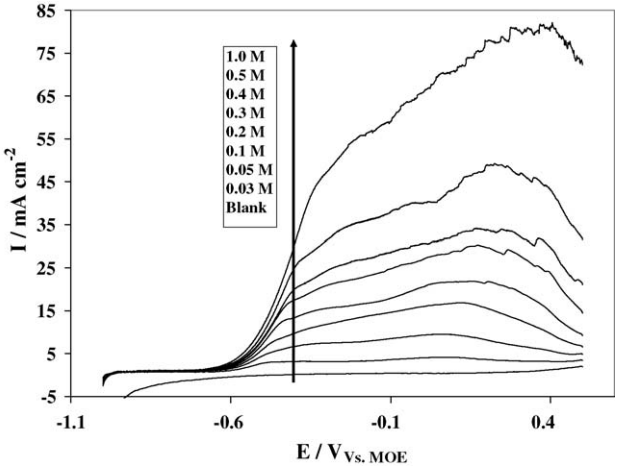

Fig. 3. Linear voltammetry of BH_4^- on colloidal Au immobilized on GC with Nafion® 117: the effect of BH_4^- concentration. Inset legend indicates the $NaBH_4$ concentration in 2 M NaOH. Scan rate 100 mV s^{-1}, 298 K.

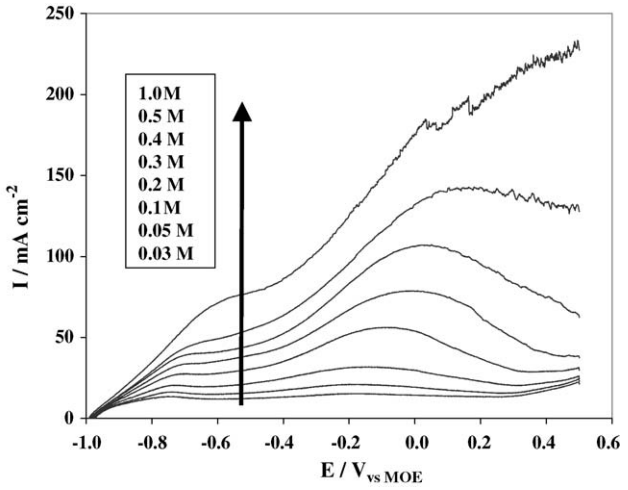

Fig. 4. Linear voltammetry of BH_4^- on colloidal Au-Pt immobilized on GC with Nafion® 117: the effect of BH_4^- concentration. Inset legend indicates the $NaBH_4$ concentration in 2 M NaOH. Scan rate 100 mV s^{-1}, 298 K.

Fig. 4 shows the voltammogram of $NaBH_4$ on Au-Pt. Two waves can be distinguished, the first one between about −0.85 and −0.6 V versus MOE is due to the oxidation of H_2 generated in the catalytic hydrolysis of $NaBH_4$ (Eq. (4)), while the second wave commencing at about −0.5 V versus MOE is given by the direct oxidation of BH_4^- on the alloy [5,9].

With Pd as a co-catalyst the voltammetry response was quite complex, composed of three distinguishable peaks depending on the borohydride concentration (Fig. 5). For comparison, Fig. 6 shows the voltammogram of BH_4^- on pure Pd. Comparing Figs. 3, 5 and 6, i.e., on pure Au, Au-Pd and pure Pd, respectively, it can be concluded that on the Au-Pd alloy, features are retained from both metals. At potentials more negative than −0.1 V versus MOE the response resembles that on Au mostly, while at more positive potentials the peak observed on Pd between −0.1 V and +0.1 V versus MOE is also apparent in the case of the alloy.

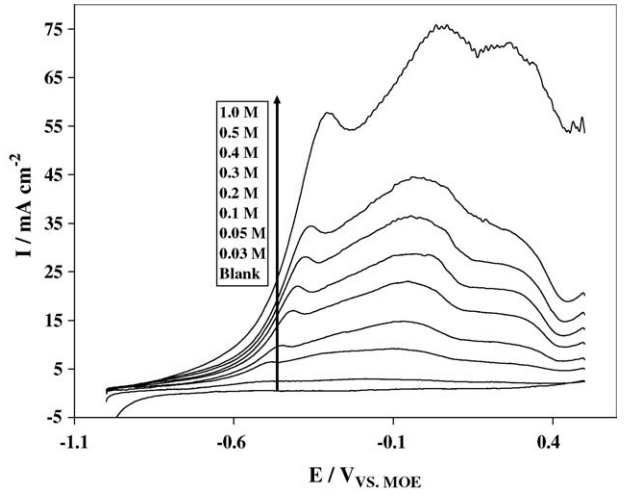

Fig. 5. Linear voltammetry of BH_4^- on colloidal Au-Pd immobilized on GC with Nafion® 117: the effect of BH_4^- concentration. Inset legend indicates the $NaBH_4$ concentration in 2 M NaOH. Scan rate 100 mV s^{-1}, 298 K.

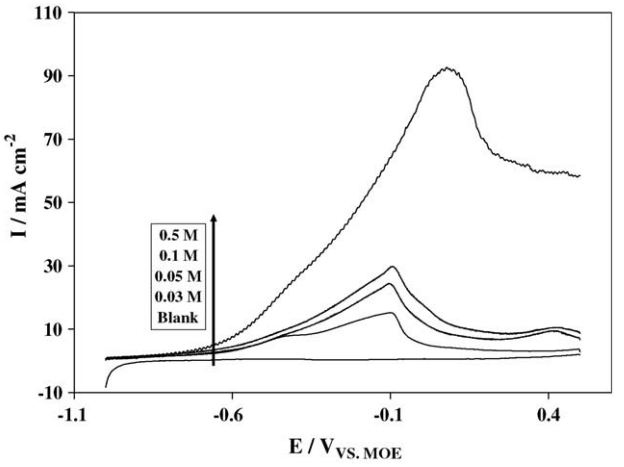

Fig. 6. Linear voltammetry of BH_4^- on colloidal Pd immobilized on GC with Nafion® 117: the effect of BH_4^- concentration. Inset legend indicates the $NaBH_4$ concentration in 2 M NaOH. Scan rate 100 mV s^{-1}, 298 K.

Among the investigated metals (Figs. 3–5), the highest superficial current densities for BH_4^- oxidation were obtained on Au-Pt suggesting an enhanced catalytic activity.

The $NaBH_4$ concentration dependence of the peak current densities corresponding to the oxidation peaks situated between −0.1 V and +0.1 V versus MOE, was linear for the three catalysts (Fig. 7). Furthermore, the same peak current densities increased linearly with the square root of scan rate (Fig. 8). Thus, it can be concluded that on the immobilized colloidal catalysts the voltammetry behaviour of the peak between −0.1 and +0.1 V versus MOE was consistent with the irreversible oxidation of a bulk species under mixed kinetic and diffusion control [14].

3.2. Voltammetry of borohydride oxidation on rotating electrodes

To study the effect of mass transfer on the effective borohydride oxidation rate, linear voltammetry at a scan rate of 5 mV s^{-1} was performed on the colloidal catalyst layer immobilized onto a rotating glassy carbon disk electrode (see Section

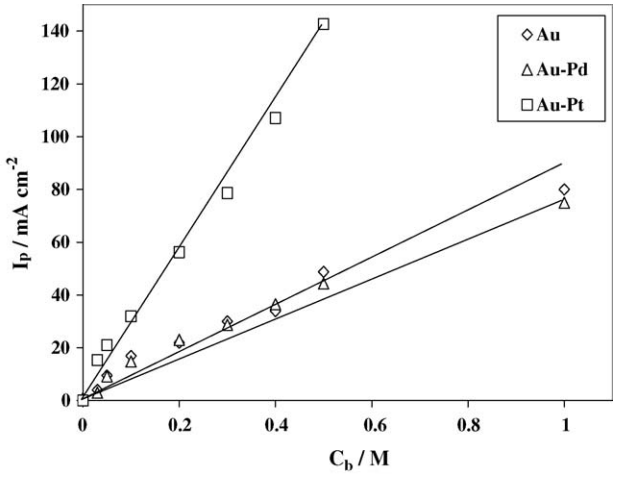

Fig. 7. The concentration dependence of the peak current density on colloidal Au and Au-alloys. Scan rate 100 mV s^{-1}, 298 K.

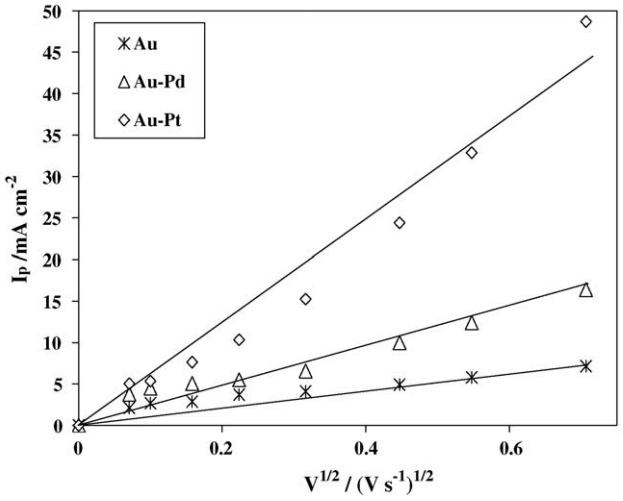

Fig. 8. The scan rate dependence of the peak current densities obtained on the colloidal Au and Au-alloys catalysts: $NaBH_4$ concentration 0.03 M (Au-Pd, Au-Pt) and 0.3 M (Au), 298 K.

2.2). The rotation rate was varied between 500 and 3000 rotations per min (rpm), the $NaBH_4$ concentration was constant at 0.3 M, and the temperature was controlled at 298 and 313 K, respectively. The rotating disk set-up simulates to some extent the operation of the anode catalyst layer in the fuel cell subjected to the convective flow of the alkaline $NaBH_4$ solution.

Fig. 9 exemplifies the experimental results obtained with the rotating electrode for the Au-Pt catalyst. Increasing the temperature from 298 to 313 K increased more than two-fold the peak current density indicating a strong kinetic effect on the voltammogram. The effect of rotation rate on the other hand, was less pronounced than what would be expected for convective mass transfer control according to the Levich equation [14].

These results suggest that the convective mass transfer of BH_4^- from the bulk solution to the outer surface of the catalyst layer was fast compared to the intra-catalyst layer diffusion of BH_4^- to the active sites. At electrode potentials more positive than the peak potential, −0.1 V versus MOE (Fig. 9), the BH_4^- depletion inside the porous catalyst structure gains significance and the intra-catalyst layer diffusion of BH_4^- could become the overall rate-limiting step. Therefore, in the time frame of the scan, enhancing the external convective flow by increasing the rotation rate of the electrode has a relatively minor influence on the overall oxidation rate. The polarization behaviour of the porous catalyst layer is likely due to the combined effect of intra-catalyst layer diffusion, electrode kinetics and possibly ionic conductivity effects. The combination of these factors typically yield the so-called multiple-Tafel slope behaviour of porous electrodes [15,16]. Extraction of quantitative information from the obtained polarization curves, such as the apparent Tafel slope and intrinsic diffusion coefficient, can be only attempted in conjunction with modeling of the flooded electrode. More detailed experimental and modeling studies are required in order to characterize quantitatively the operation of the porous anode in borohydride fuel cells.

3.3. Chronopotentiometry

Chronopotentiometry is a useful qualitative catalyst screening method since it simulates the constant current operation of a fuel cell. Fig. 10 shows both the open circuit and the anode potential at 10 mA cm^{-2} for the investigated Au and Au-alloys catalysts. The reversible potential for the complete eight-electron oxidation of BH_4^- according to reaction (1) under the conditions of Fig. 10 is −1.41 V versus MOE (i.e., −1.28 V versus SHE). The open circuit potentials (OCP) measured deviate from the reversible potential of the BO_2^-/BH_4^- couple, e.g., the OCP was −0.97 V versus MOE for Au-Pt and −0.64 V versus MOE for Au (Fig. 10). The open circuit values are essentially mixed potentials with contributions potentially from species such as dissolved O_2, H_2 generated during catalytic hydrolysis on Pt and Pd, and possibly various boron hydroxides formed in the hydrolysis reaction.

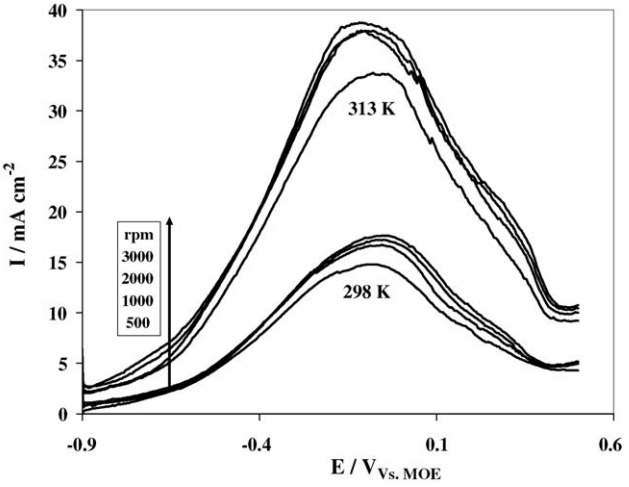

Fig. 9. Linear voltammetry of BH_4^- oxidation on colloidal Au-Pt catalysts immobilized on a rotating GC disk electrode: the effect of rotation rate and temperature. Scan rate 5 mV s^{-1}, 298 and 313 K. $NaBH_4$ concentration 0.3 M in 2 M NaOH. Inset legend indicates the rotation rate per min.

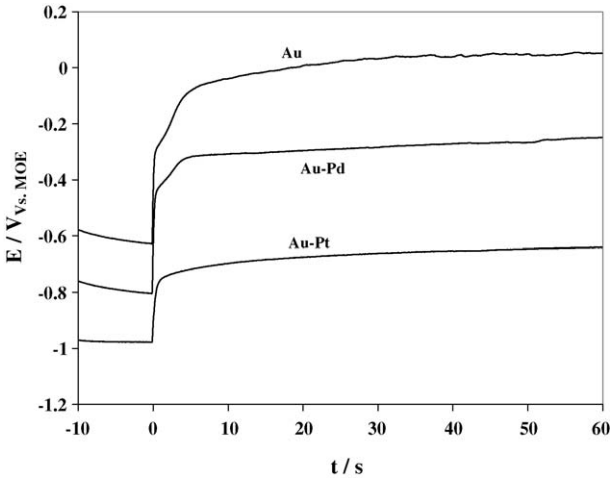

Fig. 10. Chronopotentiometry of BH_4^- oxidation on colloidal Au and Au-alloys catalysts. Current step: from 0 to 10 mA cm^{-2}. 0.5 M $NaBH_4$ in 2 M NaOH; 298 K.

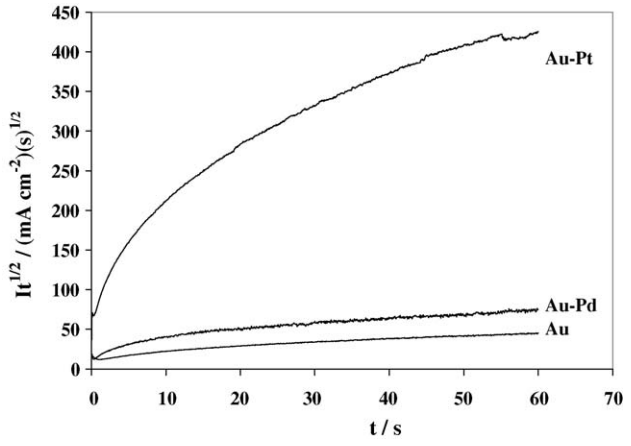

Fig. 11. Cottrell plot generated from the chronoamperometry data in the case of a potential step from −0.9 to −0.2 V vs. MOE.

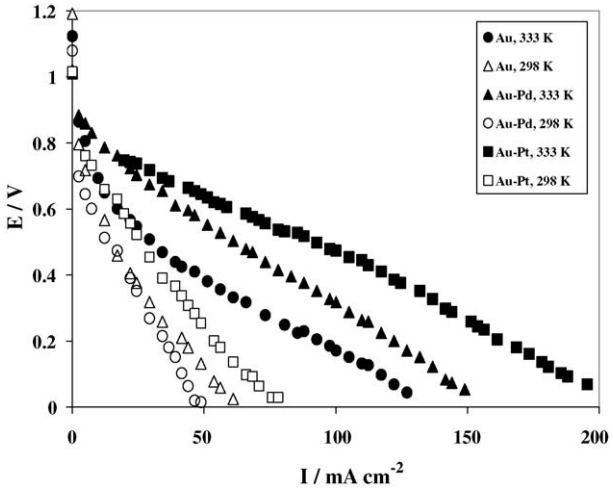

Fig. 12. Borohydride fuel cell polarization curves at 298 K and 333 K: Comparison between the colloidal Au and Au-alloys catalysts. Anode catalyst load 5 mg cm^{-2}; 85 ml min^{-1} 2 M $NaBH_4$–2 M NaOH. Cathode catalyst (Pt) load 4 mg cm^{-2}. O_2 flow rate 200 ml min^{-1} at 2.7 atm (abs).

For a superficial current density of 10 mA cm^{-2} the lowest overpotentials were measured on Au-Pt, followed by Au-Pd and then Au. Therefore, both alloys outperformed Au under the employed chronopotentiometry conditions (Fig. 10).

3.4. Chronoamperometry

In chronoamperometry experiments, the potential was stepped from −0.9 to −0.2 V versus MOE, which is virtually the most positive anode potential at which the fuel cell would operate in practice. The chronoamperometry results obtained for the +0.7 V potential step are summarized as a Cottrell plot in Fig. 11.

The highest anodic current densities for all the potential steps were measured on Au-Pt followed by Au-Pd and lastly by Au, corroborating therefore, the chronopotentiometry results regarding the activity series. On the most active catalyst, i.e., Au-Pt, $i\cdot\sqrt{t}$ increased with time. The borohydride oxidation rate at −0.2 V versus MOE is high on Au-Pt, thus, BH_4^- is consumed at the outer edge of the catalyst layer, at the bulk electrolyte solution–catalyst layer interface and neither the intra-catalyst layer diffusion nor the external mass transfer of BH_4^- does not become rate limiting under the employed conditions. Furthermore, the increase of the $i\cdot\sqrt{t}$ function is also an indication that the electrode surface is not poisoned during the time course of the experiment.

In the case of Au on the other hand, the virtual constancy of the $i\cdot\sqrt{t}$ versus t after about 20 s of operation (Fig. 11), could be attributed to electrode deactivation since diffusion control, a typical cause of constant $i\cdot\sqrt{t}$ versus t plot, could be ruled out based on the lower catalytic activity of Au compared to Au-Pt.

3.5. Fuel cell performance

Fuel cell experiments were performed at 298 and 333 K, using the colloidal Au, Au-Pt and Au-Pd anode catalysts, in membrane electrode assemblies (MEA) of 5 cm^2 effective area equipped with a commercial cathode Pt catalyst (4 mg cm^{-2}) and Nafion® 117 membrane (see Section 2.3).

Fig. 12 shows the fuel cell polarization curves obtained using the colloidal Au, Au-Pt and Au-Pd catalysts at 298 and 333 K, respectively. The cell equipped with the Au anode catalyst had the highest open circuit voltage (OCV), e.g., 1.2 V at 298 K, compared to about 1 V obtained with Au-Pt, apparently contradicting the findings in chronopotentiometry showing a higher open circuit potential for Au-Pt (Fig. 10). However, as noted in Section 3.3, the open circuit anode potentials measured in chronopotentiometry were mixed potentials, while in the fuel cell setup using the cation exchange membrane the crossover of fuel (BH_4^-) and/or oxidant (O_2) is reduced. The open circuit cell voltage values for the Pt and Pd alloys (i.e., 1 V) are likely affected on the anode side by the presence of H_2 generated in-situ by the catalytic hydrolysis of BH_4^-, thus resembling the H_2–O_2 fuel cell.

Furthermore, Fig. 12 shows that the largest operating cell voltages were obtained with the Au-Pt anode catalyst, e.g., 0.47 V at 100 mA cm^{-2} and 333 K. Under identical conditions the Au anode catalyst yielded only 0.17 V.

Unfortunately, no direct comparison can be made with the work of Amendola et al. [4] since in the latter work the Au catalyst load has not been specified, the anode design is different and furthermore, an anion exchange membrane has been used.

Figs. 13–15 show the combined effect of temperature and anolyte flow rates on the cell polarization curves obtained for Au, Au-Pt and Au-Pd catalysts, respectively. It is important to emphasize that the open circuit cell voltage was generally higher the lower the anolyte flow rate (e.g., using Au at 298 K the OCV was 1.28 V at a flow rate of 20 ml min^{-1}, while 1.19 V was obtained at 85 ml min^{-1}). This indicates that the cation exchange membrane does not completely eliminate the BH_4^- crossover from the anode to the cathode in spite of a 2.7 atm (abs) O_2 pressure. Consequently, the higher the anolyte flow rate the higher the crossover rate, lowering the cell voltage due to the establishment of a mixed potential on the cathode.

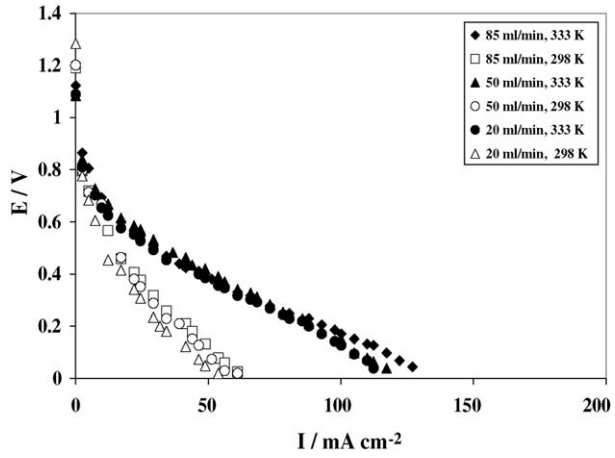

Fig. 13. Effect of anolyte flow rate on the borohydride fuel cell polarization curves using Au anode catalyst. Anode catalyst load 5 mg cm^{-2}; 2 M $NaBH_4$–2 M NaOH. Cathode catalyst (Pt) load 4 mg cm^{-2}. O_2 flow rate 200 ml min^{-1} at 2.7 atm (abs).

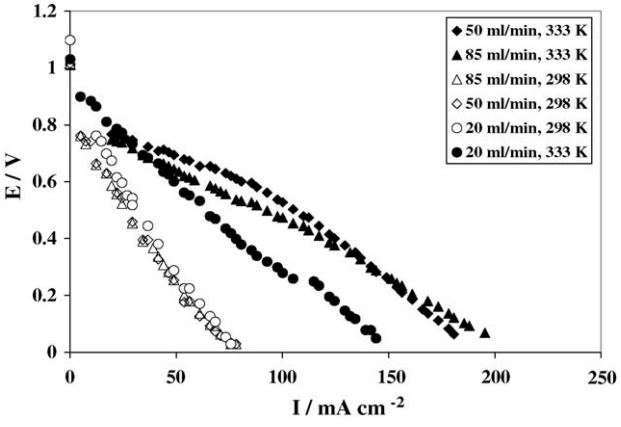

Fig. 14. Effect of anolyte flow rate on the borohydride fuel cell polarization curves using Au-Pt anode catalyst. Anode catalyst load 5 mg cm^{-2}; 2 M $NaBH_4$–2 M NaOH. Cathode catalyst (Pt) load 4 mg cm^{-2}. O_2 flow rate 200 ml min^{-1} at 2.7 atm (abs).

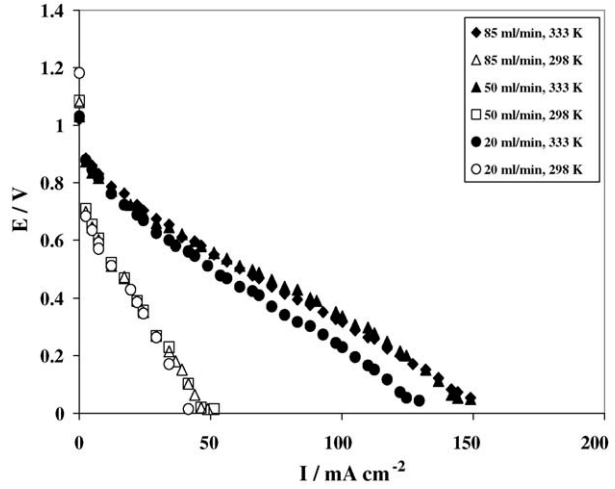

Fig. 15. Effect of anolyte flow rate on the borohydride fuel cell polarization curves using Au-Pd anode catalyst. Anode catalyst load 5 mg cm^{-2}; 2 M $NaBH_4$–2 M NaOH. Cathode catalyst (Pt) load 4 mg cm^{-2}. O_2 flow rate 200 ml min^{-1} at 2.7 atm (abs).

From Figs. 13–15, it is clear that at 298 K the anolyte flow rate in the investigated range of 20–85 ml min^{-1} had a negligible effect in all cases on the fuel cell polarization curves confirming therefore, the RDE results which suggested the lesser importance of convection compared to intra-catalyst layer diffusion. At 333 K on the other hand, for Au-Pt (Fig. 14) increasing the flow rate above 20 ml min^{-1}, improved the cell voltage at superficial current densities higher than 50 mA cm^{-2}. This finding is consistent with the discussion presented in relation to the chronoamperometry results (Section 3.4) where it was emphasized that on Au-Pt, due to the high activity, the reaction front is located at the outer edge of the catalyst layer, i.e., the bulk solution/catalyst layer interface. Therefore, at temperatures greater than 298 K and superficial current densities above 50 mA cm^{-2}, improving the convective mass transfer to the catalyst layer increased the fuel cell voltage by decreasing the anode concentration overpotential.

4. Conclusions

In this study supported Au, Au-Pd and Au-Pt (1:1 atomic ratio) nano-particles were prepared according to the Bönneman method and their electrocatalytic activity toward borohydride oxidation was investigated. Fundamental electrochemical studies performed on supported colloidal catalysts immobilized on glassy carbon substrate, showed that alloying Au with Pd or Pt improves the electrode kinetics of $NaBH_4$ oxidation. Fuel cell experiments conducted with an anode catalyst load of 5 mg cm^{-2} in a cation exchange membrane-gas diffusion electrode arrangement using a 2 M NaOH–2 M $NaBH_4$ solution, revealed that the Au-Pt anode catalyst gave the highest operating cell voltages, e.g., 0.47 V at 100 mA cm^{-2} and 333 K. In a complementary follow up study Pt and Pt-Ir were investigated as catalysts for borohydride oxidation and compared with the performance of Au-Pt [5].

Future studies should investigate in detail whether a particle size effect is also operative in the case of borohydride electrooxidation in addition to the mechanistic and kinetic differences between the Au and Pt electrodes as shown previously [9]. It is estimated based on literature regarding the Bönneman method that alloying the relatively large colloidal Au with Pt or Pd would reduce the mean particle size from about 10 nm for pure Au [11] to about 6 nm. The role, if any, played by the particle size difference between the pure Au and its Pt and Pd alloys should be further studied.

Acknowledgements

The authors gratefully acknowledge funding from the Natural Sciences and Engineering Research Council of Canada, the British Columbia Advanced Systems Institute and The University of British Columbia new faculty start-up grant.

References

[1] Z.P. Li, B.H. Liu, K. Arai, K. Asaba, S. Suda, J. Power Sources 126 (2004) 28.

[2] B.H. Liu, Z.P. Li, K. Arai, S. Suda, Electrochim. Acta 50 (2005) 3719.
[3] N.A. Choudhry, R.K. Raman, S. Sampath, A.K. Shukla, J. Power Sources 143 (2005) 1.
[4] S.C. Amendola, P. Onnerud, M.T. Kelly, P.J. Petillo, S.L. Sharp-Goldman, M. Binder, J. Power Sources 84 (1999) 130.
[5] E.L. Gyenge, M.H. Atwan, D.O. Northwood, J. Electrochem. Soc. (2005) in press.
[6] B.S. Richardson, J.F. Birdwell, F.G. Pin, J.F. Jansen, R.F. Lind, J. Power Sources 145 (2005) 21.
[7] Z.P. Li, B.H. Liu, K. Arai, S. Suda, J. Electrochem. Soc. 150 (2003) A868.
[8] M.V. Mirkin, H. Yang, A.J. Bard, J. Electrochem. Soc. 139 (1992) 2212.
[9] E. Gyenge, Electrochim. Acta 49 (2004) 965;
E. Gyenge, Electrochim. Acta 49 (2004) 1875.
[10] M.H. Atwan, D.O. Northwood, E.L. Gyenge, Int. J. Hydrogen Energy 30 (2005) 1323.
[11] H. Bönneman, K.S. Nagabhushana, J. N. Mater. Electrochem. Syst. 7 (2004) 93.
[12] M. Götz, H. Wendt, Electrochim. Acta 43 (1998) 3637.
[13] R.I. Masel, Chemical Kinetics and Catalysis, Wiley-Interscience, New York, 2001, pp. 667–755 and 837–880.
[14] E. Gileadi, Electrode Kinetics for Chemists, Chemical Engineers and Material Scientists, Wiley-VCH, New York, 1993, p. 413 and 85.
[15] M.L. Perry, J. Newman, E.J. Cairns, J. Electrochem. Soc. 145 (1998) 5.
[16] E.L. Gyenge, J. Power Sources, in press (Published on-line April 13, 2005).